Upper crustal structure of central Java, Indonesia, from transdimensional seismic ambient noise tomography

Z. Zulfakriza,[1] E. Saygin,[2] P. R. Cummins,[2] S. Widiyantoro,[3] A. D. Nugraha,[3] B.-G. Lühr[4] and T. Bodin[5]

[1] *Earth Sciences Graduate Program, Faculty of Earth Sciences and Technology, ITB, Bandung,* 40132, *Indonesia. E-mail:* zulfakriza@students.itb.ac.id
[2] *Research School of Earth Sciences, The Australian National University, Canberra ACT* 0200, *Australia*
[3] *Global Geophysics Research Group, Faculty of Mining and Petroleum Engineering, ITB, Bandung,* 40132, *Indonesia*
[4] *GFZ German Research Centre for Geosciences, Telegrafenberg, Potsdam D-*14473, *Germany*
[5] *Berkeley Seismological Laboratory, University of California at Berkeley, Berkeley, California* 94720, *USA*

SUMMARY

Delineating the crustal structure of central Java is crucial for understanding its complex tectonic setting. However, seismic imaging of the strong heterogeneity typical of such a tectonically active region can be challenging, particularly in the upper crust where velocity contrasts are strongest and steep body wave ray paths provide poor resolution. To overcome these difficulties, we apply the technique of ambient noise tomography (ANT) to data collected during the Merapi Amphibious Experiment (MERAMEX), which covered central Java with a temporary deployment of over 120 seismometers during 2004 May–October. More than 5000 Rayleigh wave Green's functions were extracted by cross-correlating the noise simultaneously recorded at available station pairs. We applied a fully non-linear 2-D Bayesian probabilistic inversion technique to the retrieved traveltimes. Features in the derived tomographic images correlate well with previous studies, and some shallow structures that were not evident in previous studies are clearly imaged with ANT. The Kendeng Basin and several active volcanoes appear with very low group velocities, and anomalies with relatively high velocities can be interpreted in terms of crustal sutures and/or surface geological features.

Key words: Seismic tomography; Crustal structure; Asia.

1 INTRODUCTION

Like much of the Indonesian archipelago, central Java has a complex and active geological setting. Its tectonic history suggests the crust is composed of several blocks accreted to the southeast Asian margin in the Cretaceous (Smyth *et al.* 2007; Hall 2009). Geodetic studies have established central Java as an area of active deformation that it is traversed by the southeastern edge of the stable Sundaland block (Simons *et al.* 2007), although this boundary is poorly defined.

Recent and ongoing tectonic activity is also reflected by overpressured crustal fluids, evidenced by mud volcanoes (Clements *et al.* 2009), as well as active volcanoes such as Mt Merapi, Mt Merbabu, Mt Sundoro and Mt Sumbing. In addition, central Java is traversed by fault systems such as the Lasem Fault, as well as the Opak River Fault system, which in 2006 experienced a disastrous shallow Mw 6.3 earthquake close by. Finally, the Java trench to the south of central Java is an active subduction zone with a convergence rate of 67 mm yr^{-1} (Simons *et al.* 2007).

Both the complicated tectonic history and the active tectonic processes can be studied using images of subsurface velocity structure produced using seismic tomography (Koulakov *et al.* 2007; Wagner *et al.* 2007) and seismic attenuation tomography (Bohm *et al.* 2013). Koulakov *et al.* (2007, 2009) have shown that very pronounced velocity anomalies, up to 30 and 36 per cent for *P* and *S* velocities, respectively, characterize the crust of central Java. These anomalies are strongest in the upper crust, at depths of 5–10 km, but anomalies as strong as 10 per cent persist to depths of 25 and 35 km.

The concentration of strong velocity contrasts at shallow depth is not surprising. Tectonic uplift and subsidence can result in the juxtaposition of deeply sourced, high-velocity crustal material with basins filled with recently deposited, low-velocity sediments and volcanic tuffs. Rapid sedimentation can lead to pronounced low velocities due to the overpressuring of fluid-saturated sediments. While the strongest signature of recent tectonic processes may be at shallow depth, the typically steep seismic ray paths used in body wave tomography may result in poor resolution at shallow depth. On the other hand, failing to account for such structure can result in 'bleeding' of the shallow velocity anomalies into tomographic images of deeper structure.

In this paper, we show how ambient noise tomography (ANT) can image the strong velocity gradients in the uppermost crust that characterize central Java. We seek to determine to what extent images obtained using ANT are compatible with conventional body wave tomography, and to what extent they provide new information that is missed by body wave tomograms. The strong velocity gradients result in strong focusing and defocusing effects (i.e. ray bending), which can result in very uneven sampling. We account for the prounced bending of ray paths using a fast marching eikonal solver (Rawlinson & Sambridge 2004), and deal with uneven sampling by using a 'transdimensional' Bayesian method that allows the model parametrization to adapt to the data coverage. We show that this method produces better images of the strong variations in subsurface velocity structure than conventional ANT.

2 DATA

We use seismic recordings collected by MERAMEX, a joint Indonesian–German temporary seismometer network operated for 150 d from 2004 May to October to study the characteristics of a volcanic system as part of an active convergent continental margin (Koulakov *et al.* 2007).

The network consisted of 134 stations, with 106 short period and 14 broad-band Güralp seismometers, eight ocean bottom hydrophones and six ocean bottom seismometers. Signals from the three-component short-period seismometers (Mark L4-3D and Güralp CMG40T) were recorded by Earth Data loggers with a sampling frequency of 100 Hz. The broad-band stations were operated with Güralp seismometers (CMG3T and CMG3ESP) and recorders (SAM; see Koulakov *et al.* 2007; Wagner *et al.* 2007). In this study, 120 land-based short-period and broad-band stations (Fig. 1) are used to extract Green's functions from available station pairs. The remaining ocean bottom seismometers were not used in the analyses.

3 AMBIENT NOISE CROSS-CORRELATIONS

Cross-correlation of noise signals between pairs of simultaneously recording receivers was first used in helioseismology to estimate the impulse response of the Sun (Duvall *et al.* 1993). Similarly, coherent information on Earth structure can be extracted by cross-correlating the vertical and horizontal components of noise records between pairs of stations (Shapiro & Campillo 2004; Sabra *et al.* 2005; Shapiro *et al.* 2005). Green's functions thus obtained can be used to image the velocity structure of a medium (Snieder 2004). Recently, tomography using Rayleigh waves extracted from empirical Green's functions estimated using cross-correlations of ambient seismic noise has been applied successfully in several regions: New Zealand (Lin *et al.* 2007), Australia (Saygin & Kennett 2010, 2012), North America (Pawlak *et al.* 2011), Tibet (Li *et al.* 2009) and the British Isles (Nicolson *et al.* 2012), and imaging of magma chambers of Lake Toba in Indonesia (Stankiewicz *et al.* 2010). These studies mapped low and high-velocity anomalies associated with large sedimentary basins and igneous and metamorphic structures, respectively.

In this study, we followed the data processing procedure of Saygin & Kennett (2010). To extract vertical-component Rayleigh wave Green's functions, we divide daily records for each station into 1-hr segments with 900 s overlap to compute the cross-correlations between pairs of stations. Cross-correlation operations are
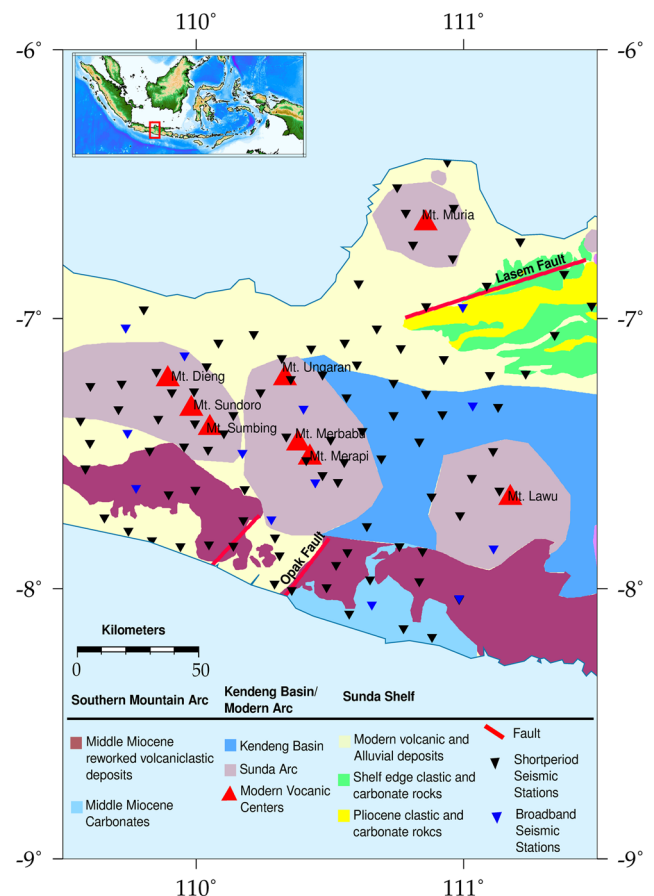

Figure 1. Map of geological features (modified from Smyth *et al.* (2008)) and the MERAMEX seismic stations that were operated around central Java–Indonesia, 106 short-period seismometers (black triangles), 14 broad-band seismometers (blue triangles). Red triangles show the location of volcanoes. Studied area (red box) is shown in the index map.

performed in the frequency domain between all possible station pairs and all available daily records. We then stack cross-correlation segments to create a daily estimate. Over 5000 Rayleigh wave Green's functions were extracted from the available data. The group velocity curves are extracted by applying a narrow-band Gaussian filter to every Green's function. The traveltimes of Green's functions were picked manually at different periods after filtering between 0.5 and 20 s. The extracted Rayleigh wave Green's functions from seismic noise cross-correlations as a function of the interstation distance is given in the Supporting Information (Fig. S1).

4 TOMOGRAPHIC INVERSION

The observed traveltimes can be inverted in a tomographic algorithm to produce 2-D maps of Rayleigh wave group velocities at each discrete frequency. Here, we use a fully non-linear inversion approach cast in a Bayesian (i.e. probabilistic) framework. As opposed to standard tomographic schemes, where the goal is to find a single best-fitting model that is dependent on a number of user-defined parameters (e.g. parametrization, regularization), here the solution is a full probability distribution that accounts for the non-uniqueness of the problem. The target distribution is defined through Bayes Theorem as the probability of the model given the observed data, namely the posterior distribution (Bayes 1958; Tarantola & Valette 1982).
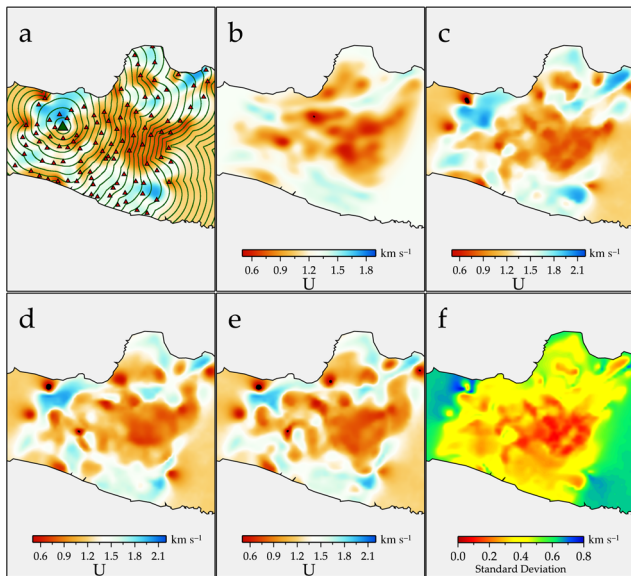
Figure 2. The rj-McMC algorithm is used in conjunction with fast marching eikonal solver to build an iterative tomography that takes into account ray bending. At each iteration, the algorithm produces a solution model for the next iteration. (a) Wave front propagation in heterogeneous media with FMM for velocity model at 5 s. A green triangle marks the location of the source. (b) Linearized inversion with starting ray geometry generated from constant velocity of 1.2 km s^{-1}. (c) rj-McMC with constant velocity of 1.2 km s^{-1}. (d) rj-McMC with ray geometry updated with velocity model from (c). (e) rj-McMC with ray geometry updated with velocity model from (d). (f) Standard deviation of the tomogram in (c).

This framework allows us to forego the use of tuning parameters that usually need to be defined using 'trial and error' procedures. For example, the complexity of the solution (number of parameters) can be treated as an unknown to be determined by the data. In this way, the number of cells used to define the unknown velocity field is not fixed in advance, but is a free parameter to be inverted for. Transdimensional inference (where the dimension of the model is variable), has been recently introduced onto the Earth sciences by Malinverno (2002), and applied to a wide range of problems (e.g. Hopcroft *et al.* 2009; Piana Agostinetti & Malinverno 2010; Gallagher *et al.* 2011; Bodin *et al.* 2012a).

Here, we sample the posterior probability function with the reversible jump Markov chain Monte Carlo algorithm (rj-McMC) Green (1995, 2003), as implemented in Bodin & Sambridge (2009) and Bodin *et al.* (2012b). The algorithm is based on a direct parameter search scheme, where a large number of individual models with variable parametrizations are tested against the data. At each step of the Markov chain, a model is proposed and either 'accepted' or 'rejected' in the ensemble solution. A property of the algorithm is that the final ensemble of accepted models is distributed according to the target distribution. The expected earth model can then be derived by simply averaging the ensemble of collected models.

Since this method requires testing a large number of models against the data, it is much more computationally expensive than conventional linearized procedures. However, it appears to be a powerful tool in relatively small problems, such as 2-D regional ANT (e.g. Young *et al.* 2013). The method presents a number of advantages: (1) The algorithm adapts to the non-even distribution of the information present in the data. (2) The solution is probabilistic, which enables rigorous quantification of uncertainties (see Fig. 2f).

(3) The Bayesian formulation can be expanded to include the data noise, that is, the required level of data fit, as a free parameter (Bodin *et al.* 2012b). For more details about transdimensional tomography, we refer the reader to Bodin & Sambridge (2009) and Bodin *et al.* (2012b).

The algorithm solves the tomographic problem for a given fixed geometry of rays. We first assume straight rays between pairs of stations to obtain an initial solution. The model thus obtained is used to update ray geometries with the fast marching Method (FMM) to solve eikonal equation (Rawlinson & Sambridge 2004). The process can be iterated a number of times to account for ray bending (i.e. focusing and defocusing effects), and we have displayed results for three such iterations in this paper.

Results for each step for 5 s period are shown in Figs 2 (c)–(e). In total, we run three iterations to update the ray path geometries successively at each period. Although the general features of the tomograms in Figs 2(c)–(e) are similar, there are some differences in boundaries of the low and high-velocity anomalies. For each period, we run rj-McMC in parallel Markov chains, one on each of 240 processors. Each of the parallel Markov chains uses 50 000 burn-in steps (to assure convergence), and another 50 000 steps to sample the parameter space. We used priors for the noise parameter and group velocity that were uniform in the ranges 0.1–5.0 s and 0.1–2.3 km s^{-1}, respectively, and considered every 100th model in each chain to avoid dependent samples in the ensemble solution.

The difference between tomographic results using conventional (subspace method, see Saygin & Kennett 2012) least-squares and transdimensional Bayesian inversion is illustrated by comparing Figs 2(b) and (e)–(f). The results in Fig. 2(e) are much more detailed than (b), and the standard deviation in (f) tells us that these details are significant. While the level of detail in the conventional inversion result could be increased by decreasing the damping and smoothing (see Figs S9 and S11), this would tell us little about which details are statistically significant. Moreover, while the number of cells used in the Bayesian inversion varies from 2 to 1000, the Bayesian framework naturally favours the simplest models that fit the data (MacKay 2003), so we can be confident that the level of detail in Fig. 2(e) is actually required by the data.

5 RESULTS AND DISCUSSION

Following the inversion procedure described above, we produced Rayleigh wave group velocity tomograms for periods between 2 and 12 s, a representative sample of which are shown in Fig. 3. Periods beyond 12 s had too few ray paths justifying computation of tomograms. Rayleigh wave group velocity sensitivity kernels calculated for representative 1-D velocity profiles indicate that, for up to 10 s period, these maps are dominated by structure at 5 km depth or less, where body wave tomography exhibits poor resolution (Koulakov *et al.* 2007). Periods of 10 s or greater are also sensitive to structure at up to 8 km depth.

The most prominent feature of all the tomograms displayed in Fig. 3 is the irregularly-shaped low-velocity anomaly underlying the volcanic arc and extending from just east of Mt Dieng to Mt Lawu. This is a pronounced low-velocity anomaly, with minimum group velocity less than 1 km s^{-1} at all periods. Because it is centred between Mt Merapi and Mt Lawu, and its prominence in the tomograms from 2 to 12 s periods suggests it extends to mid-crustal depths, this strong and pervasive anomaly seems consistent with the Merapi–Lawu Anomaly (MLA) identified by Koulakov *et al.* (2007). However, because the MLA in our tomograms weakens at
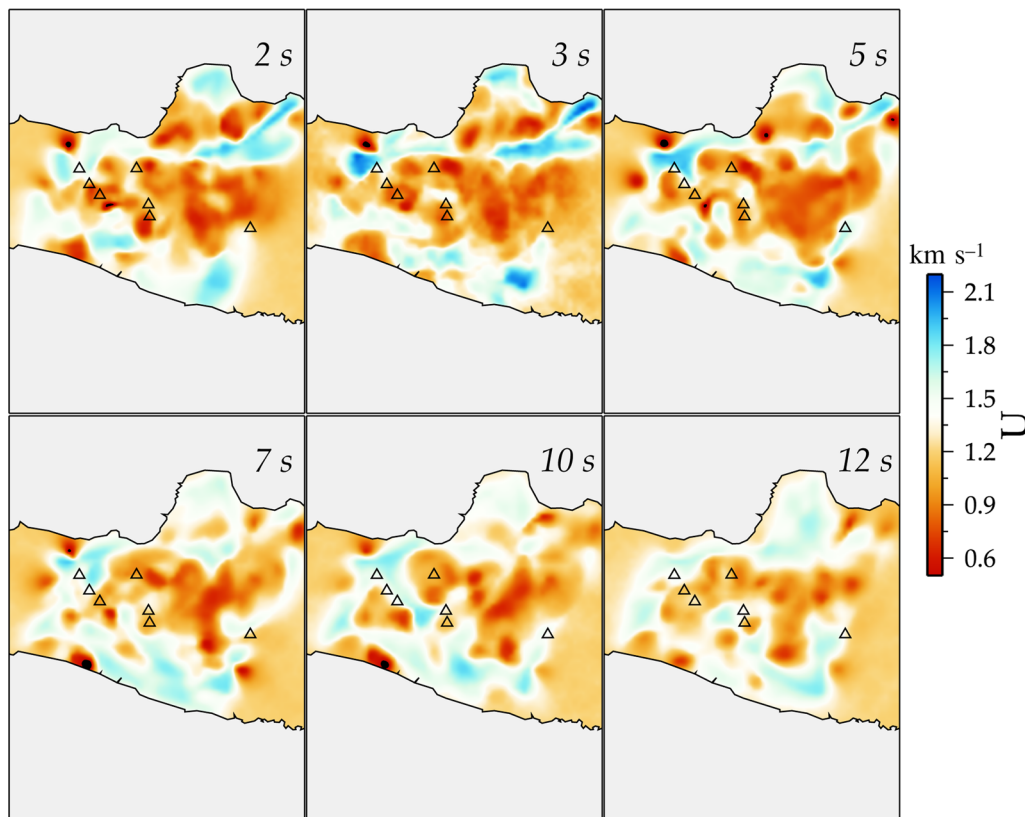
Figure 3. Inversion results, expressed as the mean of the posterior distribution obtained from rj-McMC sampling, for Rayleigh wave group velocities U between 2 and 12 s shown in map view. Locations of the active volcanoes are given with black triangles.

12 s period, we believe the anomaly is concentrated in the upper 5 km of the crust.

Koulakov *et al.* (2007) estimated the ratio of *P*- and *S* velocities (*Vp/Vs*) to ascribe the low velocities of the MLA to the presence of fluids and partial melt, but noted the difficulty in distinguishing between this and low-velocity sediments that fill the Kendeng Basin overlying the MLA. Due to the sensitivity of our ANT tomograms to shallow structure, this is probably more true for our results—that is, although our results for the MLA show a stronger concentration of low-velocity material in the shallow crust, it is more difficult to say how much of this is due to the presence of fluid or partial melt, and how much is due to the sediments filling the Kendeng Basin.

Another feature prominent in our tomograms from 2 to 5 s period appears as a relatively high group velocity anomaly that has a roughly linear shape, extending along an SW–NE direction and intersecting the northern coast of Java near the upper right corners of the top panels in Fig. 3. This feature underlies the Rembang High, and its position and orientation suggest that it lies along the suture between the Mesozoic 'Sundaland Core' and terranes of arc and ophiolitic material accreted to its southeastern edge in the late Cretaceous (Hall 2009). The high velocity, at least relative to the MLA, is likely due to the presence of shallow marine clastic and extensive carbonate sedimentary rocks along the Palaeogene Sunda Shelf in the 2–6 km depth range (Smyth *et al.* 2008). In the 2 and 3 s tomograms, this anomaly appears to be 'mirrored' by a similar anomaly about 20 km to the southeast, although this later feature is much weaker at longer periods. It is worth noting that this feature was not evident in the body wave tomography results of Koulakov *et al.* (2007), possibly because it is limited to shallow depth, where the body waves have poor resolution.

Finally, a third feature evident in all the tomograms but more prominent in those for periods greater than 10 s, corresponding to mid-crustal depths, is the relatively high group velocity extending along the coast of southern Java. A similarly positioned high-velocity anomaly is discernible in both the *P*- and *S*-velocity results of Koulakov *et al.* (2007), where it is shown to extend to at least 15 km depth. It is tempting to suggest that this may represent the fragment of Gondwana continental crust postulated by Smyth *et al.* (2007) to lie beneath the south coast of eastern Java on the basis of zircon dates. However, it may be that these relatively high group velocities correspond to 'normal' values of Rayleigh wave group velocity, that simply appear high because they are juxtaposed with the extremely low group velocities of the MLA to the north.

6 CONCLUSIONS

We extracted Green's functions by cross-correlating seismic noise from available station pairs in central Java, Indonesia using the MERAMEX data set. Retrieved Rayleigh waves contain energy in the period range of 1 to 18 s, and arrival times of these surface waves were picked for the available station pairs (see Fig. S1). Tomographic images derived from the inversion of the group wave velocity of Rayleigh waves clearly depict pronounced group velocity contrasts delineating some of the major geological structures in the upper crust beneath central Java. These structures are dominated by a strong negative group velocity underlying the volcanic arc and the Kendeng sedimentary basin, surrounded by relatively high group velocities that may represent crustal blocks accreted to the Sundaland core in the late Cretaceous.

We have established that ANT applied to dense deployments of seismometers is an effective means for imaging the strongly

heterogeneous structure in the upper crust in active tectonic regions such as central Java. We find that the uppermost (until 5 km depth) crust in this region is characterized by variations of 30–40 per cent about an average Rayleigh wave group velocity lower than $1.5 \, \mathrm{km \, s^{-1}}$.

The large velocity contrasts encountered in this study will present challenges for the determination of 3-D crustal velocity models, but we believe approaches such as full waveform inversion of the Green's functions (Fichtner *et al.* 2013) may be applicable and will be the focus of future work. The determination of this 3-D structure will be important for improving tomographic images of the deeper crust using body and surface wave data.

ACKNOWLEDGEMENTS

REFERENCES

Bayes, T., 1958. An essay towards solving a problem in the doctrine of chances, *Biometrika,* **45,** 295–315 [reprint of the original article which appeared in *Philos. Trans. R. Soc. Lond.*, 1763, **53,** 370–418].

Bodin, T. & Sambridge, M., 2009. Seismic tomography with the reversible jump algorithm, *Geophys. J. Int.,* **178**(3), 1411–1436.

Bodin, T., Salmon, M., Kennett, B.L.N. & Sambridge, M., 2012a. Probabilistic surface reconstruction from multiple data sets: an example for the Australian Moho, *J. geophys. Res.,* **117,** B10307, doi:10.1029/2012JB009547.

Bodin, T., Sambridge, M., Rawlinson, N. & Arroucau, P., 2012b. Transdimensional tomography with unknown data noise, *Geophys. J. Int.,* **189,** 1536–1556.

Bohm, M., Haberland, C. & Asch, G., 2013. Imaging fluid-related subduction processes beneath Central Java (Indonesia) using seismic attenuation tomography, *Tectonophysics,* **590,** 175–188.

Clements, B., Hall, R., Smyth, H.R. & Cottam, M.A., 2009. Thrusting of a volcanic arc: a new structural model for Java, *Petrol. Geosci.,* **15,** 159–174.

Duvall, T.L., Jefferies, S.M., Harvey, J.W. & Pomerantz, M.A., 1993. Time–distance helioseismology, *Nature,* **362,** 430–432.

Fichtner, A., Trampert, J., Cupillard, P., Saygin, E., Taymaz, T., Capdeville, Y. & Villaseñor, A., 2013. Multiscale full waveform inversion, *Geophys. J. Int.,* **194,** 534–556.

Gallagher, K., Bodin, T., Sambridge, M., Weiss, D., Kylander, M. & Large, D., 2011. Inference of abrupt changes in noisy geochemical records using transdimensional changepoint models, *Earth planet. Sci. Lett.,* **311,** 182–194.

Green, P., 1995. Reversible jump MCMC computation and Bayesian model selection, *Biometrika,* **82,** 711–732.

Green, P., 2003. Trans-dimensional Markov chain Monte Carlo, *High. Struct. Stoch. Syst.,* **27,** 179–198.

Hall, R., 2009. The Eurasian SE Asian margin as a modern example of an accretionary orogen, *Geol. Soc. Lond. Spec. Publ.,* **318,** 351–372.

Hopcroft, P., Gallagher, K. & Pain, C., 2009. A Bayesian partition modelling approach to resolve spatial variability in climate records from borehole temperature inversion, *Geophys. J. Int.,* **178**(2), 651–666.

Koulakov, I. *et al.*, 2007. P and S velocity structure of the crust and the upper mantle beneath central Java from local tomography inversion, *J. geophys. Res.,* **112,** B08310, doi:10.1029/2006JB004712.

Koulakov, I., Jakovlev, A. & Luehr, B.G., 2009. Anisotropic structure beneath central Java from local earthquake tomography. *Geochem. Geophys. Geosyst.,* **10,** Q02011, doi:10.1029/2008GC002109.

Li, H., Su, W., Wang, C.Y. & Huang, Z., 2009. Ambient noise Rayleigh wave tomography in western Sichuan and eastern Tibet, *Earth planet. Sci. Lett.,* **282,** 201–211.

Lin, F.C., Ritzwoller, M.H., Townend, J., Bannister, S. & Savage, M.K., 2007. Ambient noise Rayleigh wave tomography of New Zealand, *Geophys. J. Int.,* **170,** 649–666.

MacKay, D.J., 2003. *Information Theory, Inference and Learning Algorithms,* Cambridge Univ. Press.

Malinverno, A., 2002. Parsimonious Bayesian Markov chain Monte Carlo inversion in a nonlinear geophysical problem, *Geophys. J. Int.,* **151**(3), 675–688.

Nicolson, H., Curtis, A., Baptie, B. & Galetti, E., 2012. Seismic interferometry and ambient noise tomography in the British Isles. *Proc. Geol. Assoc.,* **123**(1), 74–86.

Pawlak, A., Eaton, D.W., Bastow, I.D., Kendall, J.M., Helffrich, G., Wookey, J. & Snyder, D., 2011. Crustal structure beneath Hudson Bay from ambient-noise tomography: implications for basin formation, *Geophys. J. Int.,* **184,** 65–82.

Piana Agostinetti, N. & Malinverno, A., 2010. Receiver function inversion by trans-dimensional Monte Carlo sampling, *Geophys. J. Int.,* **181**(2), 858–872.

Rawlinson, N. & Sambridge, M., 2004. Multiple reflection and transmission phases in complex layered media using a multistage fast marching method, *Geophysics,* **69**(5), 1338–1350.

Sabra, K.G., Gerstoft, P., Roux, P., Kuperman, W.A. & Fehler, M.C., 2005. Extracting time-domain Green's function estimates from ambient seismic noise, *Geophys. Res. Lett.,* **32,** L03310, doi:10.1029/2004GL021862.

Saygin, E. & Kennett, B.L.N., 2010. Ambient seismic noise tomography of Australian continent, *Tectonophysics,* **481,** 116–125.

Saygin, E. & Kennett, B.L.N., 2012. Crustal structure of Australia from ambient seismic noise tomography, *J. geophys. Res.,* **117,** B01304, doi:10.1029/2011JB008403.

Shapiro, N.M. & Campillo, M., 2004. Emergence of broadband Rayleigh waves from correlations of the ambient seismic noise, *Geophys. Res. Lett.,* **31,** L07614, doi:10.1029/2004GL019491.

Shapiro, N.M., Campillo, M., Stehly, L. & Ritzwoller, M.H., 2005. High-resolution surface-wave tomography from ambient seismic noise, *Science,* **307,** 1615–1618.

Simons, W.J.F. *et al.*, 2007. A decade of GPS in southeast Asia: resolving Sundaland motion and boundaries, *J. geophys. Res.,* **112,** B06420, doi:10.1029/2005JB003868.

Smyth, H.R., Hamilton, J.P., Hall, R. & Kinny, P., 2007. The deep crust beneath island arcs: inherited zircons reveal a Gondwana continental fragment beneath East Java, Indonesia, *Earth planet. Sci. Lett.,* **258,** 269–282.

Smyth, H.R., Hall, R. & Nicholas, G.J., 2008. Cenozoic volcanic arc history of East Java, Indonesia: the stratigraphic record of eruptions on an active continental margin. *Geol. Soc. Am.,* **436,** 199–222.

Snieder, R., 2004. Extracting the Green's function from the correlation of coda waves: a derivation based on stationary phase, *Phys. Rev. Lett.,* **69,** doi:10.1103/PhysRevE.69.046610.

Stankiewicz, J., Ryberg, T., Haberland, C. & Natawidjaja, D.H., 2010. Lake Toba volcano magma chamber imaged by ambient seismic noise tomography, *Geophys. Res. Lett.,* **37,** L17306, doi:10.1029/2010GL044211.

Tarantola, A. & Valette, B., 1982. Inverse problems = quest for information, *J. Geophys.,* **50,** 150–170.

Wagner, D., Koulakov, I., Rabbel, W., Lühr, B.-G., Wittwer, A., Kopp, H., Bohm, M. & Asch, G., 2007. Joint inversion of active and passive seismic data in central Java, *Geophys. J. Int.,* **164,** 218–238.

Wessel, P. & Smith, W.H.F., 1998. New, improved version of the Generic Mapping Tools Released, *EOS,* **79,** 579.

Young, M.K., Rawlinson, N. & Bodin, T., 2013. Transdimensional inversion of ambient seismic noise for 3D shear velocity structure of the Tasmanian crust, *Geophysics,* **78**(3), WB49–WB62.

SUPPORTING INFORMATION

Additional Supporting Information may be found in the online version of this article:

Figure S1 (http://gji.oxfordjournals.org/lookup/suppl/doi:10.1093/gji/ggu016/-/DC1)

Please note: Oxford University Press is not responsible for the content or functionality of any supporting materials supplied by the authors. Any queries (other than missing material) should be directed to the corresponding author for the article.